Adsorption properties of Fe-attapulgite nanocomposite removal tannin from aqueous solution

Yiqun Xu[a], Zhixin Wang[a], Xingyu Shen[b], Huixin Xiong[a],*

aCollege of Environmental Science and Engineering, Yangzhou University, Yangzhou Jiangsu 225127, China, Tel. +86 139 1213 4185; emails: huixinx@163.com (H. Xiong), qunxyq@163.com (Y. Xu), wzx18360312660@163.com (Z. Wang)
bCollege of Architectural Science and Engineering, Yangzhou University, Yangzhou Jiangsu 225127, China, email: xingyus7@163.com

ABSTRACT

Iron-modified attapulgite (Fe-ATP) was successfully prepared via a facile hydrothermal method. Their structure and properties were studied by Fourier-transform infrared spectrometer, scanning electron microscopy, X-ray diffraction. The chemical element compositions and chemical bonds of Fe-ATP were detected by X-ray photoelectron spectroscopy. The adsorption kinetics and isotherm model, the effects of adsorbent dosage, the initial pH value of the tannin solution, and contact time and temperature on the adsorption capacity of the tannin (TA) were explored. The results show that the iron modified attapulgite presented excellent adsorption. The adsorption performance of 30% Fe-ATP was the best and the adsorption capacity reaches 34.86 mg·g⁻¹. When the pH value was 3, the adsorption capacity reaches the highest 40.9 mg·g⁻¹. The above results showed that this could be attributed to the increase of surface area caused by the introduction of iron hydroxide, and electrostatic interaction may play a key role in the adsorption process. It can be concluded that Fe-ATP was suitable as an adsorbent material to remove TA from aqueous solution.

Keywords: Attapulgite; Modified attapulgite; Tannin; Adsorption properties

1. Introduction

With the wide application of tannin (TA) in pharmaceutical, food, and other industries, the discharge of tannin wastewater into the environment has caused serious environmental pollution [1–4]. Tannin is a natural organic matter widely distributed in surface water and soil. It has a well-defined structure and relatively high molecular weight (average 1,700 g·mol⁻¹) in the form of deprotonation [5]. Tannin could be toxic to aquatic organisms (algae, fish, plankton, etc.) [6]. Notably, it is the precursor of carcinogenic disinfection by-products present in drinking water [7]. Therefore, the removal of tannin from wastewater is meaningful. At present, the commonly used techniques for removing tannin from water include adsorption, coagulation, electrochemical, biological, and oxidation [8]. Owing to the advantages of high adsorption capacity, ecofriendly and recyclability, the adsorption method [9,10] regarded as a feasible approach.

In recent years, attapulgite has attracted much attention because of its unique structure and adsorption properties. Attapulgite (also called palygorskite) is a crystalline magnesium silicate hydrate mineral with an unusual lamellar chain-like crystal structure, a large number of micropore channels, and a relatively high surface area, so it has a significant adsorption capacity [11]. However, the poor dispersion and undesirability adsorption efficiency of natural attapulgite limit its application in water treatment. In

* Corresponding author.

order to improve its absorptivity, it is often modified, such as acid modification to remove impurities and increase specific surface area [12]. In addition, some metal cations are often present as anion radicals. These negative charges repel the point charges on the surface of attapulgite, leading to the weakening of the adsorption of attapulgite on metal cations [13]. It can be noted that cationic active agent can be used for modification to enhance the adsorption capacity of pollutants [14]. Therefore, attapulgite can be functionally modified in this way to improve its adsorption capacity for specific pollutants in most environments.

At present, the most widely used cationic surfactants for the removal of organic contaminants. Therefore, attapulgite (ATP) can be modified by ion exchange between a large number of cations and anions in ATP, so as to achieve the purpose of removing negatively charged pollutants from wastewater [15]. In addition, the catalytic activity and environmental function of the catalyst depending on its structure and morphological characteristics [16]. For example, Zhang et al. [17] reported a new cellulose/chitosan on adsorption of methylene blue, it presented excellent adsorption, but the material was mainly adsorbed by an amino group rather than the porous material itself. Fu et al. [18] reported a hybrid method for modifying ATP (without any purification) with 3-mercaptopropyl trimethoxy silane. These modifications are sophisticated. At the same time, iron oxide as an excellent adsorbent has received extensive attention. However, due to the aggregation and precipitation characteristics of iron oxides limit their adsorption performance to pollutants. Lin et al. [19] reported the adsorption behaviors of arsenic on the iron modified attapulgite (Fe-ATP). Iron (hydro)oxides could well disperse inside the pores and interlayers of ATP to construct the optimum metallic sites, which have good retention for arsenate. Natural attapulgite has not been purified in the above literature. The structure of iron hydroxides also needs to be clarified. In addition, the adsorption mechanism needs to be further elaborated

In this work, we successfully synthesized iron modified attapulgite. The special structure of Fe-ATP was confirmed by X-ray diffraction (XRD) and Fourier-transform infrared spectroscopy (FTIR). In addition, the surface group and morphology of ATP and Fe-ATP were characterized with FTIR and scanning electron microscopy (SEM) analyzed kinetics and isotherm models to determine the adsorption equilibrium time of pollutants and the saturated adsorption capacity of the material. In addition, the batch tests were carried out for test conditions to discuss the influence of the initial solution pH of, the adsorbent dosage, the adsorbate concentration, and the co-existing anions on the adsorption of tannin.

2. Materials and methods

2.1. Materials

The attapulgite (initial ATP) used in this experiment was purchased from Huaian Zhongao Mining Co., Ltd., (China). Sodium salt reagent (>99%) was from Sinopharm Chemical Reagent Co., Ltd., (Shanghai, China). All other solvents were obtained from the same commercial source and other solvents used were all analytical reagent grade.

2.2. Preparation of the adsorbents

The initial ATP was treated at 300°C in a muffle furnace, and after grounded into a powder. The heat-treated initial ATP was added to the 2.5 M HCl solution according to the solid-to-liquid ratio of 1:4, and stirred constantly for 2 h to remove impurities in the attapulgite pores. Ultrasound for 30 min, the sediment was washed with deionized water several times until the supernatant pH 6~7, then, it was oven dried at 105°C. The solids were milled and specified as purified attapulgite (ATP) [20].

ATP (10 g) and $FeCl_3$ with different masses were mixed, and dissolved in deionized water (50 mL), the mass ratios of ferric-soil $\left(m_{FeCl_3} : m_{ATP} \right)$ were 0.1, 0.15, 0.25, 0.3, 0.4, 0.5, 0.75, 1 respectively, and recorded as $Fe\text{-}ATP_{0.1}$ ~ $Fe\text{-}ATP_1$ [21]. Fully reacted with constant stirring at 80°C for 2 h at fixed pH 10, and aged at room temperature for 2 d. Poured off the supernatant, deionized water and ethanol were used to wash the precipitate until the sediment was nearly neutral, then it was once again oven dried at 55°C. The obtained product was Fe-ATP.

2.3. Batch adsorption experiments

0.02 g Fe-ATP with different iron-soil mass ratios (ATP as control) and the 20 mL tannin solutions (50 mg·L⁻¹) were mixed in a 50 mL centrifuge tube, placed in a thermostatic oscillator at 25°C and speed of 180 rpm (the external environment of all adsorption tests was the same). Samples were taken at 5, 10, 20, 30, 45, 60, and 90 min, centrifuged at 4,000 rpm, and the absorbance of the supernatant was measured at λ = 276 nm. Three horizontal tests were set for each sample, and the control standard deviation was not more than 5% [22].

For the adsorption isotherms, it was carried out at different temperatures (15°C, 25°C, 35°C) when the initial concentration of TA was 10~90 mg·L⁻¹. Shaked in a constant temperature oscillator for 90 min, measured the absorbance of the supernatant tannin. Langmuir and Freundlich adsorption models were used to fit the adsorption data.

2.4. Effect of pH and co-existing anions

The effects of initial pH and co-existing anions on adsorption of TA on Fe-ATP were studied over an initial pH range of 3.0~9.0 and co-existing anions (Cl⁻, NO_3^-, SO_4^{2-} and $H_2PO_4^-$) by oscillating for 90 min at 25°C. The supernatant was collected after centrifugation (4,000 rpm) and the adsorption of the TA was monitored by measuring the absorbance at λ = 276 nm. The initial pH values were adjusted to desired values with 0.10 M NaOH or HCl.

2.5. Characterization and analysis

XRD patterns were acquired on an XRD-600 X-ray diffractometer (Shimadzu, Japan), the wide-angle XRD patterns of the samples ranged from 10°–80°. FTIR spectra was carried out on a FTIR spectrometer (Nicolet 5700, Thermo Nicolet) with a spectral resolution of 4 cm⁻¹. The powder samples were prepared by grinding and pressing with KBR. The surface morphology of the materials was investigated

by scanning electron microscope (SEM, JSM-7001F, JEOL, Japan). Brunauer–Emmett–Teller (BET) values and aperture distributions were obtained using 2460 V2.01 Instrument (Micromeritics Instrument Corporation, USA). The zeta potential was determined by zeta potentiometer (ZS90). X-ray photoelectron spectroscopy (XPS) was conducted with a ESCALAB 250 (Thermo Scientific) with Mg-Kα source to determine the C, Fe, and O atoms present on the surface.

3. Results and discussion

3.1. Analysis of key characteristics

The XRD patterns of the three samples are shown in Fig. 1a. The peaks at 2θ = 19.88°, 20.90° correspond to the primary diffraction of the (040), and (121) planes of initial ATP, respectively. The XRD indicated that the heat treatment at 300°C had little effect on the crystal structure of ATP [23]. Besides, by comparing the characteristic peaks of

Fe-ATP, the degree at 11.84 and 16.79 were the characteristic peaks of iron hydroxide, indicating that was present in it. Also, Fig. 1b shows their FTIR spectra. The adsorption peaks located at 3,629 and 741 cm^{-1} in the initial ATP infrared spectrum correspond to the –OH and the O–Al bond characteristic peak of Si–O–Al [24,25]. After acid activation, the peaks at 1,455 and 876 cm^{-1} became almost disappeared. It might be the reason that the carbonate and AI–Fe–OH bonds were partially destructed during activation. This indicated that the purification process had no obvious effect on the structure of ATP but the impurity carbonate decreases obviously [26]. There was a new adsorption peak at 889 cm^{-1} in the Fe-ATP infrared spectrum, resulting from the stretching vibration of Fe–OH [27]. All these results indicated that iron hydroxide had been successfully grafted to attapulgite crystal.

Typical SEM images of samples are shown in Fig. 1c–f. Initial ATP crystals appear as rods or fibers stacked
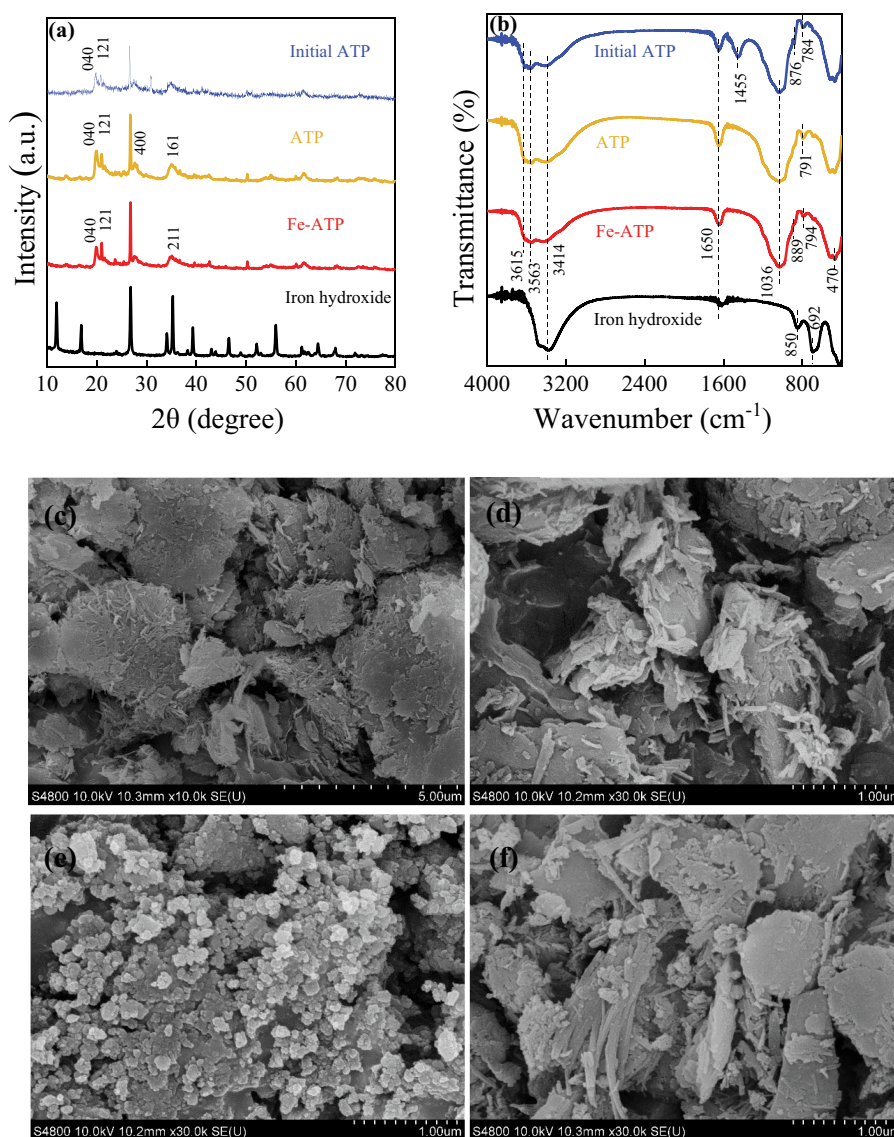
Fig. 1. XRD patterns (a), FTIR spectra (b), and SEM images (c–f) of initial ATP, ATP, iron hydroxide, Fe-ATP.

together into bundles, interspersed with sheets of associ- ated minerals. The surface morphology of ATP was obvi- ously different from that of initial ATP. Some octahedral residues support the tetrahedral sheet, which increased the number of holes and the specific surface area of ATP. Moreover, ATP crystals become compact and thin between layers, tetrahedral plates lose support, structure collapse, and internal pore channels disappeared [28]. A small number of spindle-shaped or rod-shaped iron hydroxide particles could be observed in the SEM images of Fe-ATP, indicating that modified attapulgite embedded and mixed well with iron hydroxide.

3.2. Zeta potential of Fe-ATP sample

As shown in Fig. 2, the surface charge of the sorbents was affected by solution pH to a large extent. Therefore, zeta potentials of Fe-ATP as a function of solution pH were determined in the pH range from 2 to 10. The zeta potential of the Fe-ATP sample was 3.34.
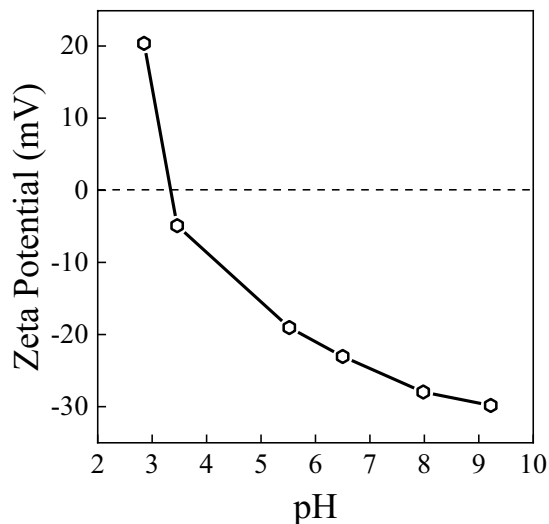
Fig. 2. Zeta potential of Fe-ATP.
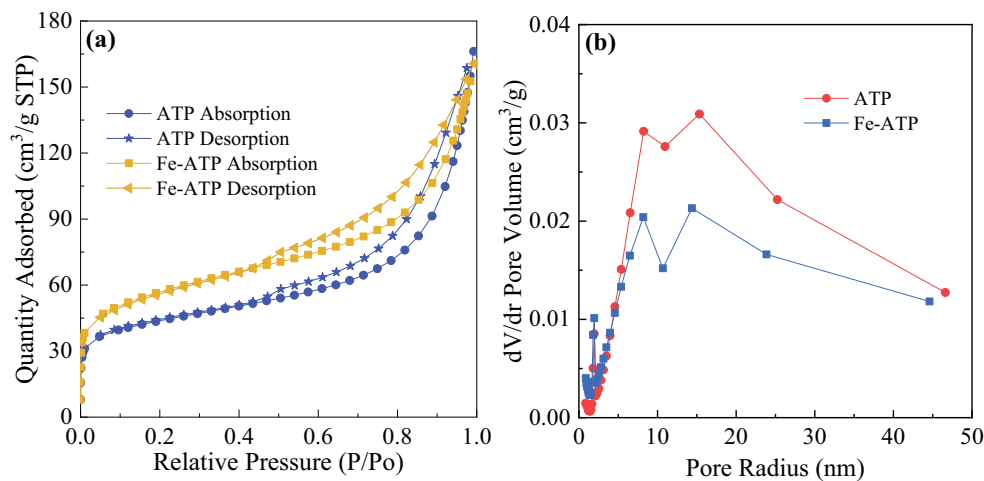
3.3. Pore structure analysis

Fig. 3a shows the N_2 adsorption–desorption isothermal adsorption curves for ATP and Fe-ATP. From the shape of the N_2 adsorption and desorption isotherms of the two car- riers, it was a typical type IV hysteresis curve, indicated that there was a strong force between the carrier and the nitrogen gas. In addition, the hysteresis loop phenome- non could be observed, which belonged to the H_3 hystere- sis loop. Further demonstrated that the nanometer material was composed of loose flake and slit shaped holes [29]. In the Barrett–Joyner–Halenda (BJH) pore size distribution curve in Fig. 3b, the distribution of 2–50 nm was the most, indicated that the number of this pore size distribution was the most. It could be concluded that ATP and Fe-ATP con- tained many micropores (pore size less than 2 nm) and a lot of mesopores (pore size between 2–50 nm).

Many researches suggested that the carbonate in ATP was removed by heat treatment and acid activation, more- over, the octahedral cations produced a certain degree of dissolution, as a result, the pore opened and the diameter of ATP was expanded, and the specific surface area was increased [30]. The pore structure parameters of Fe-ATP and ATP are shown in Table 1. It could be seen from the data that the specific surface area of the Fe-ATP increased to some degree relative to the ATP, but the pore size decreased. The increase of the specific surface was beneficial to the adsorption of TA by Fe-ATP.

3.4. Effect of contact time on adsorption kinetics

The dynamic changes of the adsorption of TA by Fe-ATP are shown in Fig. 4a. At the initial stage of adsorption, the adsorption capacity of Fe-ATP with different ferro-soil mass ratios significantly increased for TA. In addition, TA diffused to the surface of the adsorbent, created a larger concentration environment, the adsorption force was rela- tively larger, so the adsorption rate was faster. After 10 min of adsorption, the adsorption capacity of Fe-ATP exceeded 50% of the total adsorption capacity, but with the extension of time, the adsorption rate decreased and the adsorption

Fig. 3. Nitrogen adsorption–desorption isotherm (a) and BJH corresponding pore size distribution curve of purified ATP and Fe-ATP (b).

gradually reached the equilibrium state [31]. It can be seen from Fig. 4a that the adsorption effect on TA will be better when the iron loading was increased within a certain range. However, if the iron loading exceeded a certain value, it may block the ATP pores, leading to decrease in the available adsorption sites and the adsorption effect. Therefore, Fe-ATP with the iron-soil mass ratio of 0.3 was used as the adsorbent for the adsorption test, and the measured adsorption capacity of Fe-ATP was 34.86 mg·g⁻¹.

Adsorption kinetics was used to study the adsorption rate and equilibrium time of the adsorption process. From Fig. 4b and Table 2, it can be seen that the Lagergren pseudo-second-order rate equation could reasonably describe the adsorption process for the adsorption systems, and the correlation coefficient R^2 was above 0.99. The experimental measurement value at 25°C was close to the theoretical equilibrium adsorption capacity obtained by the fitting model equation. The second-order kinetic model

showed that the adsorption process depended on chemical adsorption and physical adsorption between the adsorbent and the adsorbate.

Lagergren pseudo-second-order rate equation integral formula was used to fit the relationship between the adsorption amount of TA by Fe-ATP and contact time. The relevant parameters of the fitting curve are shown in Table 2. It can be represented as:

$$\frac{t}{q_t} = \frac{1}{kq_e^2} + \frac{t}{q_e} \tag{1}$$

$$q_t = \frac{\left(C_0 - C_t\right) \cdot V}{m} \tag{2}$$

where q_t, q_e are the adsorption capacity of TA by the adsorbent at time t and equilibrium (mg·g⁻¹); C_0 and C_t were the concentration of TA in the solution at the initial time and time t of adsorption (mg·L⁻¹); V was the volume of the solution in the centrifuge tube (L); m was the dosage of adsorbent (g); K was the constant of adsorption rate.

3.5. Effect of temperatures on adsorption isotherms

The effect of the equilibrium concentration of TA on adsorption at various temperatures are shown in Fig. 5a.

Table 1
Results of the structural parameters of samples

Sample	Specific surface area (m²·g⁻¹)	Pore volume (cm³·g⁻¹)	Average pore size (nm)
ATP	141.77	0.19	5.37
Fe-ATP	190.02	0.20	4.24
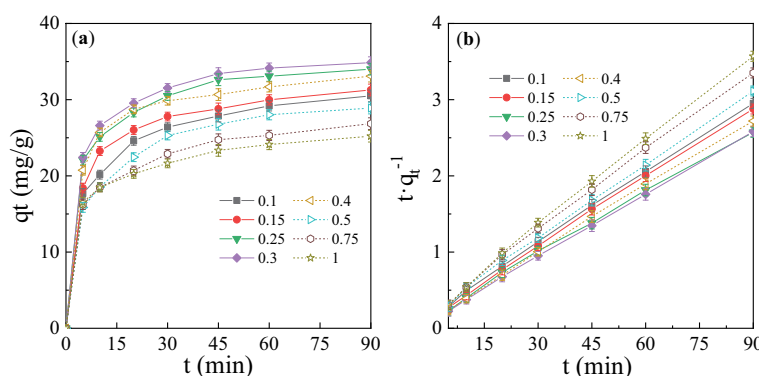
Fig. 4. Effect of contact time on adsorption, ATP and Fe-ATP (a), pseudo-second-order rate equation of TA adsorption on Fe-ATP (b). ([TA]ₐₗₗ₀ = 50 mg·L⁻¹, solution volume = 20 mL, adsorbent dose = 1 g·L⁻¹) ([TA]ₐₗₗ₀ = 50 mg·L⁻¹, solution volume = 20 mL, adsorbent dose = 1 g·L⁻¹).

Table 2
Parameters and regression coefficients for the equilibrium models for TA kinetics adsorption by Fe-ATP

Different iron-soil mass ratio Fe-ATP	Theory of Q_e (mg·g⁻¹)	Test of q_e (mg·g⁻¹)	K (mL·(mg·min)⁻¹)	R^2
Fe-ATP₀.₁	32.15	30.50	0.0054	0.9989
Fe-ATP₀.₁₅	32.57	31.27	0.0066	0.9992
Fe-ATP₀.₂₅	35.59	34.00	0.0051	0.9976
Fe-ATP₀.₃	36.23	34.86	0.0072	0.9997
Fe-ATP₀.₄	34.13	33.09	0.0077	0.9993
Fe-ATP₀.₅	30.58	28.90	0.0056	0.9984
Fe-ATP₀.₇₅	28.17	26.86	0.0062	0.9980
Fe-ATP₁	26.25	25.51	0.0079	0.9973
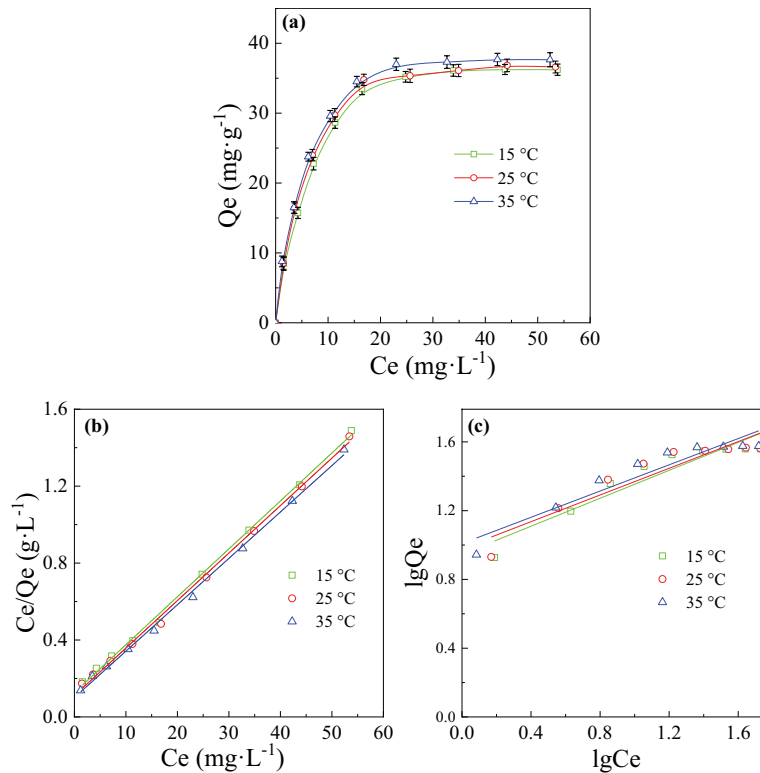
Fig. 5. Adsorption isotherms for TA by Fe-ATP (a), Langmuir (b) and Freundlich (c) adsorption isotherms model of TA by Fe-ATP (solution volume = 20 mL, adsorbent dose = 1 g·L^{-1}).

In the range of TA concentration from 10 to 90 mg·L^{-1}, the adsorption capacity of TA by Fe-ATP increased as the equilibrium concentration of TA increased until it reached equilibrium, which may be due to the high concentration gradient and driving force [32]. It could be seen that in the range of 15°C~35°C, the temperature had little effect on the adsorption capacity, so normal temperature (25°C) was selected as the test temperature.

The adsorption isotherm was the concentration relationship curve when the adsorption process of unit mass of adsorbent reached equilibrium on the two-phase interface at a certain temperature. In the present experiment, the adsorption equilibrium data were analyzed by the virtue of Langmuir and Freundlich isotherm equations.

Langmuir isotherm was perhaps the best known of all isotherms, which was often applied in describing the single-layer adsorption process of molecules with the same activation energy. It can be represented as:

$$\frac{C_e}{Q_e} = \frac{C_e}{Q_m} + \frac{1}{Q_m \times b} \tag{3}$$

where Q_m was the saturated adsorption capacity of the monolayer (mg·g^{-1}); C_e and Q_e was the concentration of adsorbate at equilibrium (mg·L^{-1}) and the adsorption capacity (mg·g^{-1}); b was a constant related to adsorption capacity (L·mg^{-1}).

The Freundlich model assumed the multilayer adsorption occurred on the non-uniform surfaces under non-ideal conditions, and it has been widely used in the

adsorption process. The linear form of the Freundlich isotherm equation was given as:

$$\log Q_e = \frac{1}{n} \log Q_e + \log K \tag{4}$$

where Q_e was the same as defined above; K was the Freundlich adsorption equilibrium constant; $1/n$ reflected the inhomogeneity of the adsorbent or the strength of the adsorption reaction.

The linear fitting results of the Langmuir model and Freundlich model at different temperatures are shown in Fig. 5b and c, and the relevant parameters are shown in Table 3. The coefficient R^2 obtained from the Langmuir isotherm equation was higher than that from the Freundlich isotherm equations. At various temperatures, the adsorption capacities determined by the Fe-ATP test were close to the theoretical adsorption capacity. According to the fitting parameters of the two models, the Langmuir model could better represent the adsorption of TA by Fe-ATP than the Freundlich model and indicate that the adsorption process was monolayer adsorption.

3.6. Effect of Fe-ATP dosage and TA concentration on adsorption

The influence of adsorbent dosage on the adsorption of TA is shown in Fig. 6a. The removal efficiency of TA improved obviously with the increase in the adsorbent dosage from 5 to 25 mg (the adsorption rate could reach 84.8%), while the adsorption capacity of the

Table 3
Parameters and regression coefficients for the equilibrium models for TA isotherm adsorption by Fe-ATP

Temperature (°C)	Langmuir model			Freundlich model		
	Q_m (mg·g^{-1})	b (L·mg^{-1})	R^2	K	n	R^2
15	40.16	0.197	0.9978	7.892	2.4612	0.8972
25	40.49	0.222	0.9975	9.563	2.5767	0.8825
35	41.49	0.238	0.9977	10.20	2.6212	0.9022
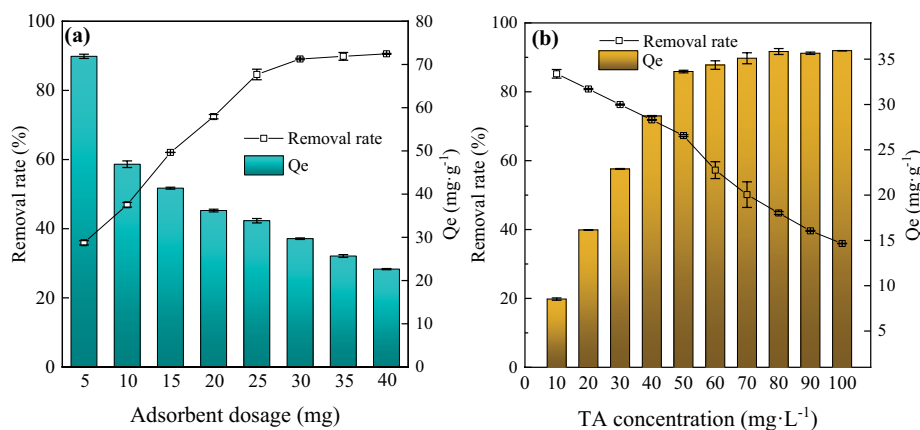
Fig. 6. Effect of adsorbent dosage on removal of TA by Fe-ATP (a), effect of TA concentration on removal of TA by Fe-ATP (b). ([TA]$_{initial}$ = 50 mg·L^{-1}, solution volume = 20 mL) (solution volume = 20 mL, adsorbent dose = 1 g·L^{-1}).

adsorbent gradually decreased. However, the adsorption rate increased slowly when the adsorbent dosage was over 25 mg. The continuous increase of adsorbent dosage dose resulted in the increase of adsorption sites. Therefore, the surface sites did not reach the adsorption saturation state, so the adsorption amount gradually decreased and the adsorption rate tended to be flat [33].

The effect of TA concentration on the adsorption is shown in Fig. 6b. As seen, the removal rate of TA decreased from 85.2% to 35.9% with the increase of TA concentration. The reason could be that as the TA concentration increased, the effective adsorption surface of the adsorbent might reach saturation, thus reduced the removal efficiency of TA. On the other hand, the adsorption capacity of TA by Fe-ATP increased from 8.52 to 33.63 mg·g^{-1} as the concentration of TA increased from 10 to 50 mg·L^{-1}, which may be due to the increased opportunities for TA to contact adsorbents with the increase of TA concentration. Thereafter, when the concentration of TA was greater than 50 mg·L^{-1}, the adsorption capacity of Fe-ATP slowly increased to 35.94 mg·g^{-1}, which may be that the active site on the surface of the adsorbent was not fully occupied when the concentration of TA was low, so the adsorption speed was fast, although the adsorption amount was low but increased rapidly. However, when the concentration of TA was increased, the adsorbent reached saturation state, and the adsorption amount tended to the equilibrium state.

3.7. Effect of initial pH and co-existing anions on adsorption

The effect of pH on the adsorption of TA by Fe-ATP is shown in Fig. 7a. It could be seen that as the pH of the

solution increases, the adsorption capacity and removal rate of the adsorbent for TA showed a decreasing trend. The adsorption capacity and removal rate of TA decreased to 30.44 mg·g^{-1} and 60.9%, respectively. The experiment showed that the adsorption effect was best when the initial pH value of TA solution was at 3. Electrostatic adsorption was one of the mechanisms affecting the adsorption process [34]. Then, the pH$_{IEP}$ of TA was determined to be 4.5, indicated that the surface charges of TA were positive or negative when the pH was below or above 4.5, corresponding. At pH < 4.5, the surface of the sample was positively charged, TA appeared as a molecule, and the coordination and reaction sites on Fe-ATP reacted with TA. However, the un-dissociated TA molecule was hydrophobic, which was easier to be adsorbed than when it exists in the form of ions due to the hydrophobic bond cooperation being used as the adsorption driving force. The adsorption of Fe-ATP was less efficient at pH > 8. It was attributed to the dissociation of the complete molecule of the TA and exists in the form of anions [35], resulting in the repulsive force between the dissociated TA and the charge with the same sign on the surfaces of the adsorbent. Thus, with the increase of pH, the TA removal rate decreases gradually.

The effect of adding Cl$^-$, NO^{3-}, SO$_4^{2-}$ and H$_2$PO$_4^-$ to the solution on the adsorption of TA by Fe-ATP is shown in Fig. 7b. The removal rates of TA were 70.0%, 69.9%, 67.0%, 68.2%, and 57.6%, respectively, when no ion (CK), Cl$^-$, SO$_4^{2-}$, NO^{3-} and H$_2$PO$_4^-$ were added. Within the allowable error range of 5%, the results demonstrate that the presence of Cl$^-$, NO^{3-}, SO$_4^{2-}$ did not significantly affect TA removal. But, H$_2$PO$_4^-$ had significant suppression of the removal of TA. This may be because Fe-ATP had high adsorption
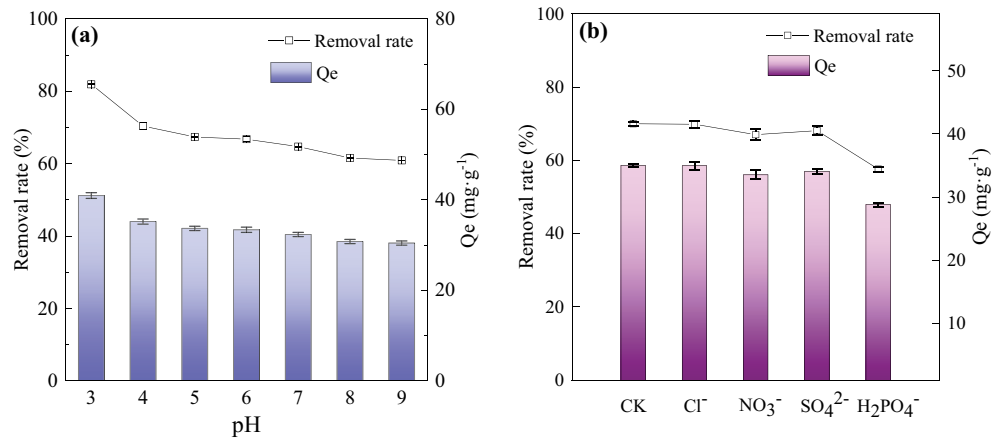
Fig. 7. Effect of pH on removal of TA by Fe-ATP (a), effect of co-existing anions on the removal of TA by Fe-ATP (b). ([TA]$_{initial}$ = 50 mg·L^{-1}, solution volume = 20 mL, adsorbent dose = 1 g·L^{-1}) ([TA]$_{initial}$ = 50 mg·L^{-1}, solution volume = 20 mL, adsorbent dose = 1 g·L^{-1}).
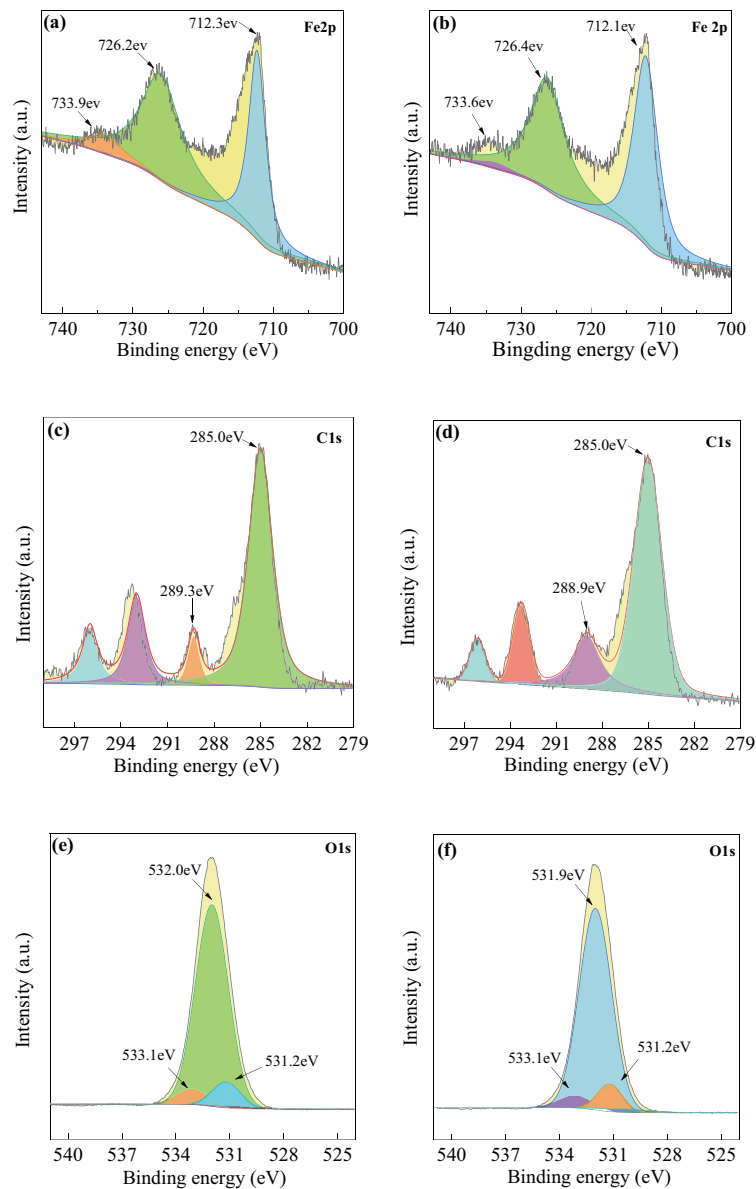
Fig. 8. XPS spectra of Fe-ATP: before Fe 2p (a), C 1s (c), O 1s (e); after: Fe 2p (b), C 1s (d), O 1s (f).

selectivity for $H_2PO_4^-$, and $H_2PO_4^-$ competed with TA for adsorption sites on the surface of the adsorbent, resulting in inhibition of TA adsorption.

3.8. XPS analysis of samples before and after adsorption

The elements contained in Fe-ATP were divided into peaks, and the analysis results are shown in Fig. 8. The XPS map of Fe 2p before and after adsorption is shown in Fig. 8a and b. The satellite peak at 733.6eV was a characteristic of Fe(Ш) in iron hydroxide, and the two peaks of Fe 2p at 726.2 and 712.3 eV were Fe $2p_{1/2}$ and Fe $2p_{3/2}$. After adsorption, TA moved to 726.4 and 712.1 eV, and the peak at Fe $2p_{3/2}$ shifted, which may be due to changes in the elemental chemical environment, indicating the formation of new chemical bonds between Fe^{3+} and other substances, and the chelation between TA and Fe [36,37].

The C 1s XPS spectra of Fe-ATP composite material are shown in Fig. 8c and d. Two peaks appear at 289.3 and 285.0 eV, belonging to O–C=O and C–C, respectively. The binding energy of C 1s may be decomposed into 285.07 eV (carbon) and 288.9 eV (standard spectrum of carbon monoxide in TA), indicating that tannic acid reacts with Fe-ATP [38].

As shown in Fig. 8e and f, the O 1s XPS spectra of Fe-ATP composites were applicable to OH–C/C=O (533.1–533.8 eV), O–C=O (532.00 eV) and C–O–Fe (531.2 or 531.7 eV), respectively. The peak at 531.9 eV was C–OH in TA. These results indicated that there was a strong interaction between ATP and iron hydroxide, and the Fe-ATP composite prepared by C–O–Fe can promote electron transfer between iron hydroxide and ATP [39].

4. Conclusions

Fe-ATP was successfully prepared in this study and assessed the stability of Fe-ATP and its performance concerning the removal of TA. Compared to ATP, The TA removal by different prepared materials followed the order of Fe-ATP > ATP > initial ATP. Fe-ATP composites with an iron-soil mass ratio of 0.3 had the highest adsorption capacity for TA and the measured adsorption capacity of Fe-ATP was 34.86 mg·g⁻¹. Discover the chelation between TA and Fe by the FTIR spectra and XPS spectrum before and after adsorption, indicated that Fe-ATP can be used as an effective adsorbent for TA removal. However, more research needs to be undertaken, because the actual removal efficiency of TA in water may also be affected by factors such as heavy metals and microorganisms.

Institutional review board statement

Not applicable.

Informed consent statement

Not applicable.

Data availability statement

Not applicable.

Conflicts of interest

The authors declare no conflict of interest.

References

[1] Z.H. Chang, Q.N. Zhang, W.Y. Liang, K. Zhou, P. Jian, G.M. She, L.Z. Zhang, A comprehensive review of the structure elucidation of tannins from *Terminalia* Linn, Evidence-Based Complementary Altern. Med., 2019 (2019) 8623909, doi: 10.1155/2019/8623909.
[2] V. Prigione, F. Spina, V. Tigini, S. Giovando, G.C. Varese, Biotransformation of industrial tannins by filamentous fungi, Appl. Microbiol. Biotechnol., 102 (2018) 10361–10375.
[3] X.Y. Sun, P. Jia, T.T. Zhe, T. Bu, Y.N. Liu, Q.Z. Wang, L. Wang, Construction and multifunctionalization of chitosan-based three-phase nano-delivery system, Food Hydrocolloids, 96 (2019) 402–411.
[4] V. Prigione, B. Trocini, F. Spina, A. Poli, D. Romanisio, S. Giovando, G.C. Varese, Fungi from industrial tannins: potential application in biotransformation and bioremediation of tannery wastewaters, Appl. Microbiol. Biotechnol., 102 (2018) 4203–4216.
[5] J. Wu, J. Chen, Adsorption characteristics of tannic acid onto the novel protonated palygorskite/chitosan resin microspheres, J. Appl. Polym. Sci., 127 (2013) 1765–1771.
[6] J. Wang, S. Zheng, J. Liu, Z. Xu, Tannic acid adsorption on amino-functionalized magnetic mesoporous silica, Chem. Eng. J., 165 (2010) 10–16.
[7] Ç. Sarıcı-Özdemir, Y. Önal, Equilibrium, kinetic and thermodynamic adsorptions of the environmental pollutant tannic acid onto activated carbon, Desalination, 251 (2010) 146–152.
[8] Q. Liang, J. Gao, D. Guo, J. Huang, J. Zhang, J. Li, B. Yang, B. Chen, Q. Wu, M. Yang, Species and formation characteristics of halogenated DBPs in chloramination of tannic acid after biodegradation, Sci. Total Environ., 781 (2021) 146690, doi: 10.1016/j.scitotenv.2021.146690.
[9] K. Ortiz-Martinez, P. Reddy, W.A. Cabrera-Lafaurie, F.R. Roman, A.J. Hernandez-Maldonado, Single and multi-component adsorptive removal of bisphenol A and 2,4-dichlorophenol from aqueous solutions with transition metal modified inorganic-organic pillared clay composites: effect of pH and presence of humic acid, J. Hazard. Mater., 312 (2016) 262–271.
[10] X. Wu, P. Gao, X. Zhang, G. Jin, Y. Xu, Y. Wu, Synthesis of clay/carbon adsorbent through hydrothermal carbonization of cellulose on palygorskite, Appl. Clay Sci., 95 (2014) 60–66.
[11] M. Suarez, J. Garcia-Rivas, E. Garcia-Romero, N. Jara, Mineralogical characterisation and surface properties of sepiolite from Polatli (Turkey), Appl. Clay Sci., 131 (2016) 124–130.
[12] H.J. Li, J.H. Xu, L.Q. Wang, D.D. Hou, Z.R. Wang, H.Z. Li, H. Hamad, Adsorption properties of modified ATP-RGO composite aerogel for removal of malachite green and methyl orange from unitary and binary aqueous solutions, Adsorpt. Sci. Technol., 2022 (2022) 1–18.
[13] J. Wen, Y. Fang, G. Zeng, Progress and prospect of adsorptive removal of heavy metal ions from aqueous solution using metal-organic frameworks: a review of studies from the last decade, Chemosphere, 201 (2018) 627–643.
[14] H. Guo, K. Xia, M. Cao, X. Zhang, Surface modification of attapulgite by grafting cationic polymers for treating dye wastewaters, Materials (Basel), 14 (2021) 792, doi: 10.3390/ma14040792.

[15] S.E. Scott, J.P. Fernandez, C.M. Hadad, A.A. MacKay, Molecular docking as a tool to examine organic cation sorption to organic matter, Environ. Sci. Technol., 56 (2022) 951–961.

[16] M.I. Afokin, I.A. Davydov, E.G. Peresypkina, M.V. Magomedova, Structure and stability of Mg-HZSM-5/Al$_2$O$_3$ catalysts for synthesizing olefins from DME: effect of thermal and hydrothermal treatments, Catal. Ind., 11 (2019) 234–242.

[17] W. Zhang, P. Sun, X. Wang, X. Zhang, L. Ran, Q. Zhao, B. Zou, L. Zhou, Z. Ye, Elevating the stability and adsorption performance of metal-organic frameworks by chitosan and attapulgite for capturing methylene blue in the water, Mater. Today Commun., 31 (2022) 103601, doi: 10.1016/j. mtcomm.2022.103601.

[18] C. Fu, X. Zhu, X. Dong, P. Zhao, Z. Wang, Study of adsorption property and mechanism of lead(II) and cadmium(II) onto sulfhydryl modified attapulgite, Arabian J. Chem., 14 (2021) 102960, doi: 10.1016/j.arabjc.2020.102960.

[19] S. Lin, H. Yang, Z. Na, K. Lin, A novel biodegradable arsenic adsorbent by immobilization of iron oxyhydroxide (FeOOH) on the root powder of long-root *Eichhornia crassipes*, Chemosphere, 192 (2018) 258–266.

[20] H. Yin, M. Kong, X. Gu, H. Chen, Removal of arsenic from water by porous charred granulated attapulgite-supported hydrated iron oxide in bath and column modes, J. Cleaner Prod., 166 (2017) 88–97.

[21] T. Luo, M. Wang, X. Tian, Y. Nie, C. Yang, H.M. Lin, W. Luo, Y. Wang, Safe and efficient degradation of metronidazole using highly dispersed β-FeOOH on palygorskite as heterogeneous Fenton-like activator of hydrogen peroxide, Chemosphere, 236 (2019) 124367, doi: 10.1016/j.chemosphere.2019.124367.

[22] J. Bialczyk, P. Natkański, P. Kuśtrowski, U. Czaja-Prokop, B. Bober, A. Kaminski, Removal of cyanobacterial anatoxin-a from water by natural clay adsorbents, Appl. Clay Sci., 148 (2017) 17–24.

[23] S. Zhang, X. Gong, Z. Shen, S. Yuan, L. Jiang, G. Wang, Study on remediation of Cd-contaminated soil by thermally modified attapulgite combined with ryegrass, Soil Sediment Contam.: An Int. J., 29 (2020) 680–701.

[24] Y. Zhu, T. Chen, H. Liu, B. Xu, J. Xie, Kinetics and thermodynamics of Eu(III) and U(VI) adsorption onto palygorskite, J. Mol. Liq., 219 (2016) 272–278.

[25] H. Wang, X. Wang, J. Ma, P. Xia, J. Zhao, Removal of cadmium(II) from aqueous solution: a comparative study of raw attapulgite clay and a reusable waste-struvite/attapulgite obtained from nutrient-rich wastewater, J. Hazard. Mater., 329 (2017) 66–76.

[26] S. Sun, X. Zeng, Y. Gao, W. Zhang, L. Zhou, X. Zeng, W. Liu, Q. Jiang, C. Jiang, S. Wang, Iron oxide loaded biochar/attapulgite composites derived *Camellia oleifera* shells as a novel bio-adsorbent for highly efficient removal of Cr(VI), J. Cleaner Prod., 317 (2021) 128412, doi: 10.1016/j.jclepro.2021.128412.

[27] X. Wei, Q. Liu, H. Zhang, Z. Lu, J. Liu, R. Chen, R. Li, Z. Li, P. Liu, J. Wang, Efficient removal of uranium(VI) from simulated seawater using amidoximated polyacrylonitrile/FeOOH composites, Dalton Trans., 46 (2017) 15746–15756.

[28] F. Meng, M. Song, Y. Chen, Y. Wei, B. Song, Q. Cao, Promoting adsorption of organic pollutants via tailoring surface physicochemical properties of biomass-derived carbon-attapulgite, Environ. Sci. Pollut. Res. Int., 28 (2021) 11106–11118.

[29] H. Pan, H. Hou, J. Chen, H. Li, L. Wang, Adsorption of arsenic on iron modified attapulgite (Fe/ATP): surface complexation model and DFT studies, Adsorption, 24 (2018) 459–469.

[30] L. Zhu, J. Qiu, W. Liu, E. Sakai, Mechanical and thermal properties of rice Straw/PLA modified by nano attapulgite/PLA interfacial layer, Compos. Commun., 13 (2019) 18–21.

[31] A. Xue, X. Zou, S. Zhou, M. Li, L. Zhu, Y. Zhao, W. Xing, C. Chen, Adsorption behaviors and mechanism of heavy metals onto attapulgite functionalized by polyamine silane, J. Am. Ceram. Soc., 104 (2020) 1887–1901.

[32] Y. Liu, Y. Kang, B. Mu, A. Wang, Attapulgite/bentonite interactions for methylene blue adsorption characteristics from aqueous solution, Chem. Eng. J., 237 (2014) 403–410.

[33] M. Litniewski, A. Ciach, Effect of aggregation on adsorption phenomena, J. Chem. Phys., 150 (2019) 234702, doi: 10.1063/1.5102157.

[34] J. Shuyue, T. Dongyan, P. Jing, Y. Xu, S. Zhaojie, Crosslinked electrospinning fibers with tunable swelling behaviors: a novel and effective adsorbent for methylene blue, Chem. Eng. J., 390 (2020) 124472, doi: 10.1016/j.cej.2020.124472.

[35] C. Peng, F. Min, L. Liu, Effect of pH on the adsorption of dodecylamine on montmorillonite: insights from experiments and molecular dynamics simulations, Appl. Surf. Sci., 425 (2017) 996–1005.

[36] L. Mei, L. Liao, Z. Wang, C. Xu, Interactions between phosphoric/tannic acid and different forms of FeOOH, Adv. Mater. Sci. Eng., 2015 (2015) 1–10.

[37] H. Guo, H. Zhang, F. Peng, H. Yang, L. Xiong, C. Wang, C. Huang, X. Chen, L. Ma, Effects of Cu/Fe ratio on structure and performance of attapulgite supported CuFeCo-based catalyst for mixed alcohols synthesis from syngas, Appl. Catal., A, 503 (2015) 51–61.

[38] L. Gao, Z. Wang, C. Qin, Z. Chen, M. Gao, N. He, X. Qian, Z. Zhou, G. Li, Preparation and application of iron oxide/persimmon tannin/graphene oxide nanocomposites for efficient adsorption of erbium from aqueous solution, J. Rare Earths, 38 (2020) 1344–1353.

[39] L. Zhang, F. Fu, B. Tang, Adsorption and redox conversion behaviors of Cr(VI) on goethite/carbon microspheres and akaganeite/carbon microspheres composites, Chem. Eng. J., 356 (2019) 151–160.